Plasma-wall interaction in Hall thrusters with magnetic lens configuration

Lubos Brieda and Michael Keidar

Citation: J. Appl. Phys. **111**, 123302 (2012); doi: 10.1063/1.4730340
View online: http://dx.doi.org/10.1063/1.4730340
View Table of Contents: http://jap.aip.org/resource/1/JAPIAU/v111/i12
Published by the American Institute of Physics.

Plasma-wall interaction in Hall thrusters with magnetic lens configuration

Lubos Brieda[a] and Michael Keidar
Department of Mechanical and Aerospace Engineering, The George Washington University, 801 22nd St., Washington, DC 20052, USA

(Received 25 October 2011; accepted 22 May 2012; published online 21 June 2012)

Some recently developed Hall thrusters utilize a magnetic field configuration in which the field lines penetrate the thruster walls at a high incidence angle. This so-called magnetic lens leads to an electric field pointing away from the walls, which is expected to reduce ion losses and improve thruster efficiency. This configuration also introduces an interesting behavior in the sheath formation. At sufficiently large angles, ions are repelled from the wall, and sheath collapse is expected. We use a plasma simulation code to investigate this phenomenon in detail. We consider the role of the magnetic field incidence angle, secondary electron emission, and a magnetic mirror. Numerical study confirms the theoretical predictions, and at large angles, ions are seen to turn away from the wall. We also consider the role of the magnetic field geometry on ion wall flux and channel erosion, and observe reduction in both quantities as the magnetic field incidence angle is increased. © *2012 American Institute of Physics*. [http://dx.doi.org/10.1063/1.4730340]

I. INTRODUCTION

Hall thrusters are spacecraft propulsion devices that utilize applied magnetic fields and closed electron Hall drift to accelerate quasi-neutral plasma. The typical Hall thruster consists of an annular or a cylindrical chamber with one end open to the ambient environment. Neutral propellant is injected through the closed end, which also contains the anode. An externally located cathode produces electrons, fraction of which enters the chamber and ionizes the propellant. In order to increase the electron transit time, and hence improve the ionization efficiency, magnetic field is applied over a section of the chamber. The magnetic field strength is selected such that electrons become magnetized and trapped in a closed azimuthal Hall drift about the thruster centerline. The magnetic field thus plays an important secondary role. Since the field restricts motion of electrons in the normal direction, electrons redistribute along the magnetic field line according to the spatial variation in ion density. The magnetic field lines thus become lines of constant potential and an electric field develops in the direction normal to the magnetic field. This electric field then in turn accelerates the ionized propellant out of the device.

In the classical Hall thruster, the magnetic field consists primarily of the radial component. Such a configuration appears ideal since it produces an electric field directed along the thruster axis. However, the presence of walls modifies the near-wall potential structure and results in a local component accelerating ions into the walls. Ion wall flux contributes to a loss of thruster efficiency and to a limited thruster lifetime due to channel erosion. In order to mitigate these losses, some recently developed Hall thrusters[1,2] have begun experimenting with magnetic fields with convex geometry. Near the walls, this so-called magnetic lens induces an electric field with a radial component directed towards the channel centerline.[3] An interesting aspect of the lens configuration is that in the vicinity of the wall, the resulting magnetic field lines can approach the wall with a highly inclined incidence angle θ, as measured from the wall normal. Such a configuration leads to an electric field with a strong radial term that, in the case of a sufficiently large θ, dominates the component due to the sheath potential drop.[4] This can be seen from a simple example. Consider a typical 300 V Hall thruster with a 200 V potential drop occurring across a 1 cm wide acceleration zone. The magnitude of the electric field $E_\perp$ is then 2×10^4 V/m. Next consider the potential drop due to the wall sheath. The electric field along the magnetic field line in the vicinity of the wall can be estimated from $E_\parallel = T_e \partial \ln n/\partial r \sim T_e/\Delta r \sim 20$ eV/0.01 cm $\sim 2 \times 10^5$ V/m.[5] Here, Δr is the sheath thickness, which is taken to be 10 Debye lengths. The angle at which the radial component of the electric field becomes negative is given by $E_r = E_\parallel \cos\theta - E_\perp \sin\theta \sim \tan\theta = E_\parallel/E_\perp$, or $\theta \sim 85^\circ$.

Ions are then accelerated away from the wall and a complete sheath collapse is expected. Although plasma-wall transition has been subject of much past research, such a research typically considered only the generalized radial case.[6] In this paper, we investigate the sheath formation and collapse in the presence of a two dimensional magnetic field. This analysis is performed using a simple axisymmetric electrostatic particle-in-cell (ES-PIC) code. We use the code to determine the structure of the plasma sheath for several magnetic field configurations. We start by investigating the response of the sheath to an inclined magnetic field. Next, we extend the analysis to include the influence of secondary electrons and a magnetic mirror. We conclude the paper with an analysis of sheath stability and channel erosion.

II. COMPUTATIONAL MODEL

A. Simulation domain

The code is based on the hybrid approach in which ions are treated as particles, but electrons are represented by a

[a]Author to whom correspondence should be addressed. Electronic mail: lubos.brieda@particleincell.com.

fluid model. The computational domain is limited to a small region near the outer wall, as illustrated in Figure 1. The small size of the computational domain allows us to resolve the Debye length and thus directly compute the electric potential in a reasonable amount of time (each simulation takes approximately 30 min). The domain captures the acceleration region characterized by the presence of strong applied magnetic field. In our formulation, the anode and the primary ionization zone are located to the left. The upper boundary represents the wall, while the bottom boundary extends into the quasineutral bulk plasma region. Ions are injected into the simulation along the left boundary and leave through the open right and bottom face or by recombining with the upper wall. The inset in Figure 1 is an example of a hybrid annular/cylindrical Hall thruster in which the magnetic field geometries of interest can be found. An example of such a device is the Princeton Cylindrical Hall Thruster[1] The highlighted box illustrates the location of the simulation domain. It should be noted that the size of the region of interest is artificially increased in this schematic drawing for clarity.

To simplify the subsequent computation, we select a simulation mesh in which the radial gridlines are aligned with the magnetic field. Such a formulation allows us to specify the necessary reference values as a function of the axial grid coordinate only. In constructing the mesh, we paid attention to two requirements. First, the mesh had to be capable of capturing the magnetic topology of interest: varying angle of magnetic field, and also the convergence of magnetic field lines in a magnetic mirror. Second, the mesh had to be suitable from the computational perspective. Particle methods require scattering of particles to the grid nodes, and conversely gathering forces by collecting values from the grid onto particle locations. Topologically structured meshes are preferred here, since physical coordinates can be mapped to the computational space via evaluation of analytical functions. The mesh shown in Figure 1 satisfies both of these requirements. The mesh coordinates are given by

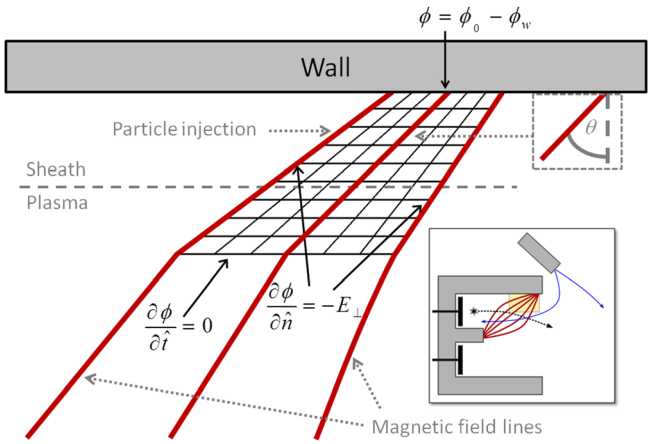

FIG. 1. Schematic of the computational domain. Ion particles are injected from the left. The inset shows a cylindrical Hall thruster and highlights the region analyzed by our code.

$$
\begin{aligned}
r &= r_0 + j * \Delta r \\
z &= i * \Delta z_j - (nr - 1 - j) * \Delta r * \tan(\theta) - 0.5 \\
&\quad * (nz - 1) * (\Delta z_j - \Delta z_w),
\end{aligned} \tag{1}
$$

where Δz_j is the local cell spacing. The cell spacing varies linearly between the top and bottom boundary. These mesh coordinates can be easily inverted. The j component is obtained first from the radial r coordinate. The i coordinate is then recovered from the axial position z using the second equation.

B. Particle injection

Xenon ions are injected into the simulation domain along the left boundary with initial velocity $u_z = u_0 + u_{th}$. Here, u_0 is the drift component and u_{th} is a random thermal velocity obtained by sampling the Maxwellian distribution function at 1 eV. The magnitude of the drift component was set to 6 km/s, corresponding to approximately 25 eV of upstream acceleration. Initial radial velocity is also obtained by sampling the random thermal component. The number of computational particles injected per time step is obtained from $p = \dot{m}\Delta t/w = n_i \bar{u} A m \Delta t/w$, where $n_i = 5 \times 10^{16}$ m^{-3} is the injection ion density and w is the macroparticle weight. The weight was selected such that cells in the bulk region contained approximately 200 computational particles at steady state. Particles were loaded with a zero azimuthal component. We assume that no forces act in the azimuthal direction and hence the cylindrical equations of motion reduce to the Cartesian form. Ion positions are updated at each time step according to the Leapfrog algorithm by integrating the Lorentz force, $\vec{F} = -e\nabla\phi$. The magnetic term is omitted, since in a Hall thruster, ions are not magnetized. Ions impacting the upper wall or leaving the computational domain were removed from the simulation. Collisions were not included as they generally play only a minor role in the sheath.

C. Potential solver

Potential was computed by solving the Poisson's equation, $\varepsilon_0 \nabla^2 \phi = -e(n_i - n_e - n_s)$, with the three densities on the right hand side corresponding to ions, primary electrons, and secondary electrons, respectively. The ion density n_i was obtained by scattering positions of kinetic ions to the computational grid. The electron density is computed from the Boltzmann equation following the approach in Refs. 7 and 8, in which the magnetic pressure effect in the presence of temperature anisotropy was considered. In the frame of reference of ions, electrons respond instantaneously to a disturbance. The time-dependent and convective terms then vanish from the momentum equation. Also, since in Hall thrusters the sheath is generally collisionless, we can disregard the collision operator. We thus arrive at the force balance,

$$
\frac{\partial}{\partial s}(n_e k T_{e\parallel}) + \frac{n_e (k T_{e\perp} - k T_{e\parallel})}{B} \frac{\partial B}{\partial s} + n_e e E_\parallel = 0. \tag{2}
$$

These terms correspond to the gas pressure, magnetic pressure, and electric field effects, respectively. Utilizing

$E_\parallel = -\partial\phi/\partial s$, the above equation can be integrated to obtain an expression for bulk electron density,

$$n_e = n_0 \exp\left[\frac{e}{kT_{e\parallel}}(\phi - \phi_0) - \frac{kT_{e\perp} - kT_{e\parallel}}{kT_{e\parallel}} \ln\left(\frac{\mathrm{B}}{\mathrm{B}_0}\right)\right]. \quad (3)$$

This is the well known Boltzmann relationship modified by the magnetic field strength term. This term is seen to reduce the electron density in regions of an increasing magnetic field—this is the magnetic mirror effect. The standard Boltzmann relationship is recovered if the magnetic field magnitude remains constant along the field lines. The magnetic pressure term also drops out if plasma is isothermal. However, as outlined in Ref. 6, Hall thruster plasma is not isothermal. In this work, we follow the results from the kinetic analysis in Ref. 6 and use $kT_{e\parallel} = 10$ eV and $kT_{e\perp} = 2kT_{e\parallel} = 20$ eV. This particular set of parameters allows us to simplify Eq. (3) further to $n_e = n_0(\mathrm{B}_0/\mathrm{B})$ $\exp[\mathrm{e}(\phi - \phi_0)/kT_{e.\parallel}]$. This simplified expression is implemented in the potential solver. It should be pointed out that this particular expression is valid only for the specific case $kT_{e\perp} = 2kT_{e\parallel}$ and a more detailed treatment would be required to consider the general case.

Equation (3) holds independently for each magnetic field line. The three constants with the 0 subscript are the reference density, potential, and magnetic field strength. These values are unique and independent along each line. We assume that electron temperature remains constant in the parallel direction, $\partial T_{e,\parallel}/\partial s = 0$, and that there is no variation in magnetic field strength in the axial direction, $\partial B/\partial z = 0$. The reference density is obtained self-consistently from the computed ion density along the bottom edge of the simulation domain, where $n_i = n_e = n_0$. A linear decay in potential is applied for majority of the cases, with $\phi_0 = \phi_L - E_\perp(\mathrm{z_w} - \mathrm{z_{w,0}})$, where $E_\perp = 20$ kV/m. Since in Hall thrusters the potential profile adjusts self-consistently based on the local discharge parameters, we also investigate an alternate cusp configuration in which the potential profile exhibits a deep valley. This setup is discussed in more detail in Sec. III D. The strength of the magnetic field is computed from the conservation of magnetic flux, $\phi_m = \int_S \vec{B}\cdot\vec{ds}$, or $Br\Delta z = C$, a constant value. Here, Δz is the cell spacing at the corresponding r value. As indicated by Eq. (3), terms relating to the magnetic strength appear only as a ratio allowing us to select an arbitrary value for the reference field.

The secondary electron density n_s is obtained from $\nabla\cdot(n\vec{u}) = 0$. Density of secondary electrons at the wall is given by $n_{s,w} = sn_{e,w}$, where $s(T_e,\theta)$ is the secondary electron emission (SEE) yield.[5] In our formulation we assume the electrons are emitted with an isotropic angular distribution and energy dependence based on the linear relationship given in Ref. 9,

$$s(T_e,\theta) \approx \sigma_0 + (1-\sigma_0)\frac{E_p}{E_1}. \quad (4)$$

For boron nitride, the typical wall material in conventional Hall thrusters, the coefficients σ_0 and E_1 are 0.54 and 40, respectively. E_p is the energy of the incoming particle, measured in eV. Initial velocity of the secondary electrons is taken to be $u_{s,w} = (2kT_w/\pi m_e)^{1/2}$. Energy conservation dictates $u = (2q\Delta\phi/m)^{1/2}$, leading to

$$n_s = sn_{e,w}\left(\frac{kT_w}{e\pi}\frac{1}{\phi - \phi_w}\right). \quad (5)$$

D. Boundary conditions

Potential along the top wall is fixed as $\phi_w = \phi_0 - \Delta\phi_W$, where the wall potential drop is given by Ref. 5 as

$$\Delta\phi_w = T_e \ln\left\{\frac{1 - s(T_e,\theta)}{v_0\left(\frac{2\pi m}{T_e}\right)}\right\}, \quad (6)$$

where v_0 is the ion velocity at the sheath edge, which in this formulation is set to the Bohm speed. The problem is closed by prescribing the normal electric field $E_\perp$ along the left and right boundaries, and zero tangential electric field $E_\parallel = 0$ on the bottom boundary. The electric field along the left and right boundaries is non-uniform for cases with a diverging magnetic field line topology. This can be seen from a simple observation of the increasing distance between field lines as one moves away from the wall. The magnitude is obtained numerically by computing the normal distance d to the next magnetic field line (grid line) at each node. The electric field is then set from $E_\perp = -\Delta\phi_0/d$. Potential is solved using the finite volume method.

E. Implementation

The simulations were performed on a domain with 50 cells in the axial and 30 cells in the radial direction. The cell spacing was set to $\sim\lambda_D = 10^{-4}$ m. Several mesh convergence studies were performed, and results obtained were found to be independent of mesh resolution at the utilized mesh spacing. The simulation time step was adjusted automatically by the code from its initial value of 1.5×10^{-9} s such that particles traveled not more than 0.33 cell lengths per time step. The wall was positioned 3 cm away from the axis. The simulation started by pre-filling the domain by injecting and propagating ion particles under the initial electric field. This fast pre-fill was found to improve the subsequent solver convergence rate. The simulation then continued in the normal mode in which the electric field was updated at each time step. The simulation continued until steady state characterized by approximately zero net change in particle counts between successive iterations. The simulation then continued for additional 2000 time steps during which results were averaged. The typical number of computational particles at steady state was 700 000. Simulation results, including potential, number densities, particle velocities, and wall fluxes were then exported. A marching squares algorithm was implemented to automatically contour the resulting velocity map to obtain the sheath boundary. In this work, we defined the sheath boundary as the contour where the radial component of velocity $v = v_B$, the Bohm

velocity. The code was implemented in the JAVA programming language and was run on a Dell Precision workstation with eight CPU cores. Each simulation was launched as an independent thread, and a simple scheduler was implemented to allow concurrent execution of the simulation cases.

III. RESULTS

A. Potential distribution at uniform density

Often we can obtain useful insight into the solution by considering a simplified case that can be evaluated in a reduced computation time. In our case, we investigated the potential distribution that forms in the presence of a completely uniform plasma. These results are illustrated in Figure 2. In all cases, plasma density of $5 \times 10^{16}\,\mathrm{m}^{-3}$ was used. The contours correspond to the lines of constant potential and the streamlines visualize the electric field. The classical Hall thruster with a solely radial magnetic field is shown in Figure 2(a). As indicated previously, this configuration results in a primarily axial electric field. However, near the wall, the sheath potential drop modifies the electric field structure such that the electric field becomes oriented towards the wall. Ions located in this near wall region are then expected to be lost to the wall recombination. Figure 2(b) illustrates what happens when the magnetic field angle is increased to 30°. Increase of the magnetic field incidence angle results in a compression of the region containing the radial electric field. Analogously, the critical streamline delineating the near wall region from the bulk acceleration zone moves closer to the wall.

Cases (c) and (d) show the effect of the magnetic lens. The net angle of the magnetic field is zero in case (c), however, the magnetic field strength decreases away from the walls. The solution is approximately antisymmetric. The electric field is seen to initially accelerate the ions away from the wall. The field subsequently acts to direct the ions back towards it. However, since ion axial velocity is increased by the electric field, the net radial deflection will be smaller in this diverging section. The predicted result is a net acceleration of ions away from the wall. Case (d) extends the magnetic mirror effect in (c) by including the 30° field inclination from (b). By comparing the electric field stream traces between cases (c) and (d), we can see that one of the effects of this combined configuration is to increase the acceleration of ions away from the wall. This effect is due to the change in the magnetic field geometry.

B. Sheath variation with magnetic field angle

We built on these initial observations by performing series of plasma simulations. We start by investigating the effect of an increasing magnetic field angle in the absence of a magnetic mirror. Secondary electron emission was not included in this set, $s = 0$ in Eq. (5). The magnetic field angle θ increased from 0° (magnetic field normal to the wall) to 85° (highly inclined configuration). Results for 0°, 40°, 60°, and 70° are plotted in Figure 3. Ion densities are shown using the contour plot. Velocity streamlines are also plotted, as well as the sheath boundary. The sheath edge is plotted by the solid red line and corresponds to the contour where the radial velocity component (i.e., the component normal to the wall) reaches the Bohm velocity $v_B = \sqrt{kT_e/m_i}$. We see that in the case of a zero magnetic field angle, the solution obtained by our code is similar to the well-known boundary layer problem. The sheath forms a short distance from the injection plane and continues to grow as more ions are accelerated from the bulk plasma towards the wall. Plasma density decrease is also influenced by the net increase in ion velocity due to the axial electric field. The result along the left boundary is somewhat non-physical, since in a real device, the sheath thickness will be finite at the entrance to the acceleration zone. Since our simulation resolves only a small subset of the Hall thruster channel, we are unable to capture the sheath that forms upstream of our domain. To investigate

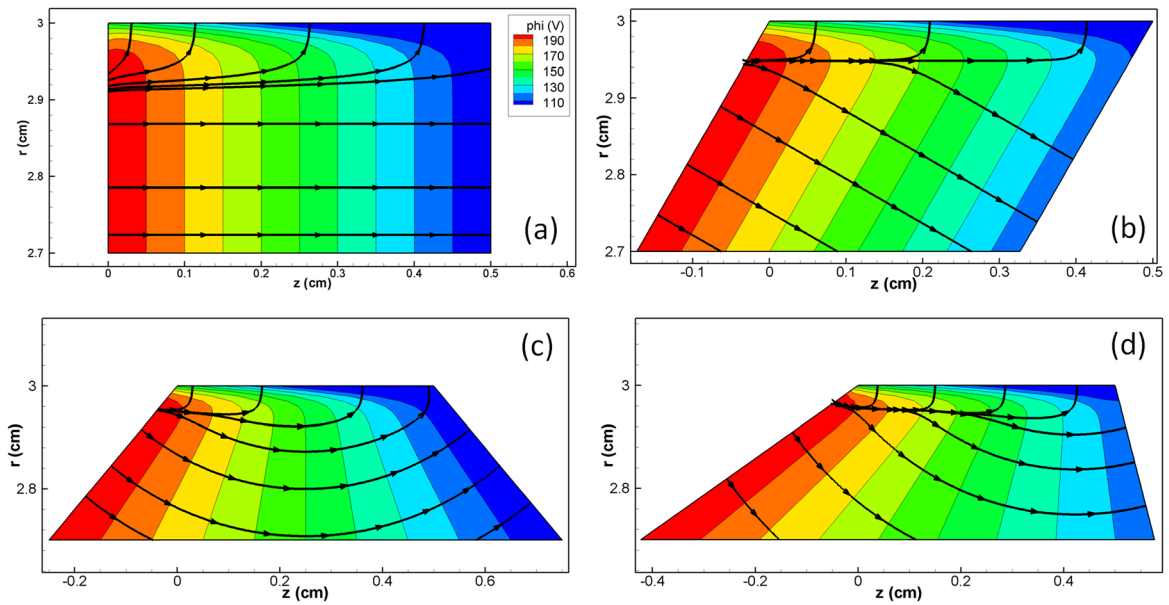

FIG. 2. Potential with uniform plasma density. (a) $\theta = 0°$, $B_w/B_0 = 1$; (b) $\theta = 30°$, $B_w/B_0 = 1$; (c) $\theta = 0°$, $B_w/B_0 = 2$; and (d) $\theta = 30°$, $B_w/B_0 = 2$.

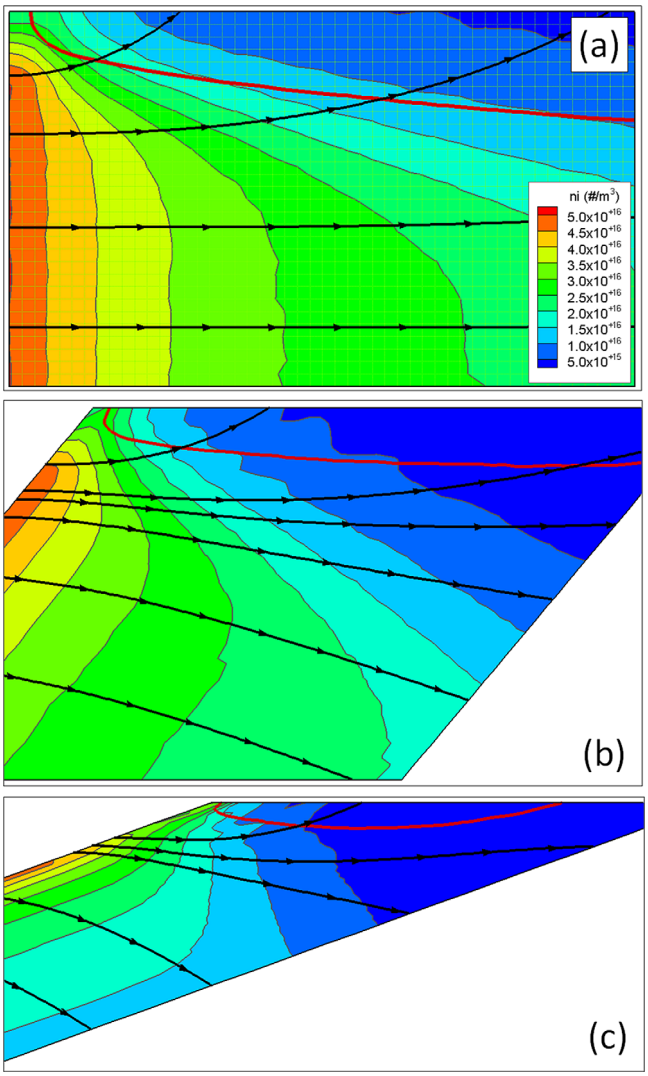

FIG. 3. Simulation results showing the ion density profile for three different magnetic field line angles, 0°, 40°, and 70°, respectively. Streamlines show ion trajectories. The red lines correspond to the sheath edge as computed with the Poisson solver.

the role the initial sheath profile has on results, we tested a modified particle loading algorithm in which the injection density decayed exponentially towards the wall. We found that differences between the two solutions were limited to several cells near the injection boundary. This finding can be explained by realizing that ions injected into the sheath will be rapidly lost to the wall. Hence, we ignore this initial region and characterize the sheath by its maximum thickness.

From our simulation, we see that the effect of an increasing magnetic field angle is to reduce the sheath thickness, as stipulated in the previous section. At 40°, the sheath thickness asymptotes to a constant value. Furthermore, ion density at the sheath edge has been reduced due to the acceleration of ions away from the wall by the electric field. At 70°, we start seeing the initial evidence of a sheath collapse. The sheath has reduced in axial size and extends only over a small section of the wall. The remaining section of the wall demonstrates a collapsed sheath. In this region, ion velocity streamlines become parallel to the wall. Instead of being accelerated into the wall, ions are seen to travel on a trajectory along the wall. This effect is not seen in configurations with a smaller magnetic field inclination angle θ.

C. Influence of secondary electron emission

We next included SEE. Secondary electron emission is an important process in SPT-type Hall thrusters, in which the acceleration channel is lined with an insulator material for which the secondary electron yield can approach unity. SEE may be an important driver in the so-called anomalous electron transport across magnetic field lines. This effect is not investigated in this work. Instead, we only concentrate on the role of SEE on the sheath profile. Same set of cases presented in the previous paragraph was run with the wall potential modified by the presence of SEE. We include secondary electrons in our code by computing the SEE emission coefficient using Eq. (4). From the wall potential relationship, Eq. (5), we can see that the presence of SEE acts to decrease the sheath potential and hence the sheath thickness. This prediction is confirmed by the result illustrated in Figure 4. This figure shows the potential contours for the 40° magnetic field inclination. The dashed lines correspond to the case with secondary electron emission. Presence of SEE is seen to reduce the sheath thickness.

D. Magnetic mirror effect

The next set of simulations was run to investigate the effect of magnetic mirror in the presence of temperature anisotropy. We used mirror ratio $R_m = B_w/B_o = 2$, and compared cases without and with a 40° magnetic field inclination. We also investigated the role of the prescribed wall potential profile. We can see from Figure 5 that the mirror plays a role similar to that of the inclined field. Convergence of field lines near the wall results in an inclined electric field analogous to the pure field rotation, Figure 3(b). We can, however, see some evidence of the defocusing effect in the diverging section. While under the pure rotation, the velocity streamlines in the bulk plasma are directed towards the channel centerline, in this configuration we see the ion trajectories follow a path parallel to the thruster axis. This is the preferred behavior, since the radial beam component does not contribute to thrust. Large plume divergence also leads to increased spacecraft contamination effects. Figure 5(b) plots the solution obtained by including a 40° magnetic field inclination and a potential "valley" that is known to occur in devices utilizing cusped magnetic profiles. In the CHT, such configurations

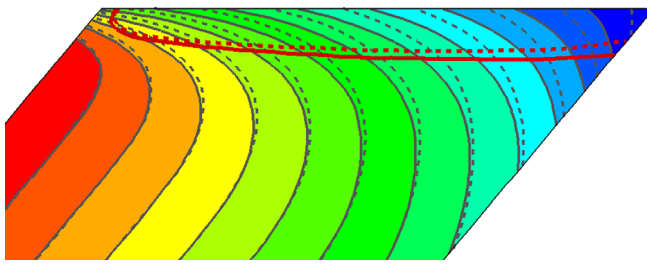

FIG. 4. Potential profile for 40°. Dashed lines indicate solution with secondary electron emission.

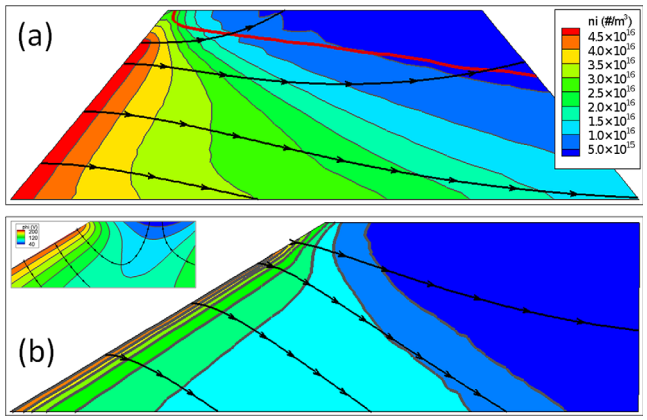

FIG. 5. Ion density contours in the presence of magnetic mirror. Magnetic mirror strength of 2 is used in both cases. Case (b) includes a 40° magnetic field inclination and a potential well. The inset shows the potential, with the contours ranging from 200 V to 40 V.

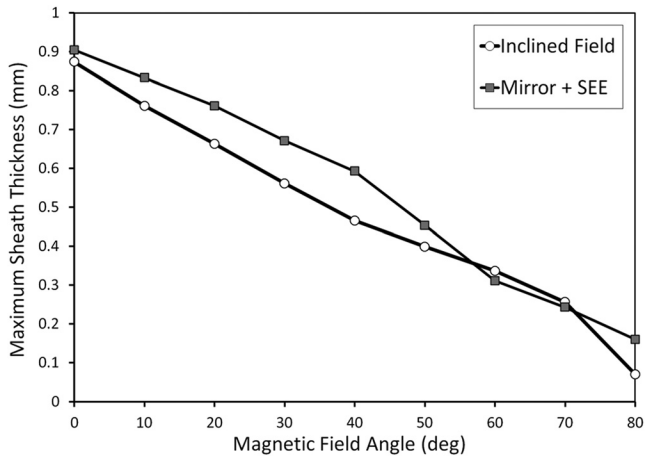

FIG. 6. Variation in the maximum sheath thickness with the angle of magnetic field. Dashed line corresponds to the solution obtained assuming quasineutrality.

arise from the difference in the physical location of the inner and outer magnets and the details of the magnetic circuitry. We modeled the potential valley by superimposing a parabolic potential drop over the linear decay, $\phi_0 = \phi_L - E_\perp(z_w - z_{w,0}) + \Delta\phi_C[4(\hat{z} - 0.5)^2 - 1]$, where $\hat{z} = (z_w - z_{w,0})/l_z$ is the normalized distance and $\Delta\phi_C = E_\perp l_z$ is the potential drop in the cusp selected to equal the potential drop in the linear region. The potential profile at steady state is shown in the inset in Figure 5(b). We see that although an electric field forms directing ions into the potential well, this profile has only negligible effect on the fast moving bulk ions. The primary effect of the potential well is to further increase the electric field accelerating the ions and ions are accelerated towards the channel centerline. It should be noted that this particular example does not take into account the dynamic nature of Hall thruster discharges. Fluctuations in the structure of the internal discharge could lead to the presence of slowly moving ions in the vicinity of the well, and these ions would subsequently be accelerated into the wall.

IV. DISCUSSION

A. Sheath collapse

In Figure 6, we plot the variation in maximum sheath thickness with the incidence magnetic field angle. We consider two cases: inclined magnetic field, and inclined magnetic field with a magnetic mirror and SEE. Linear potential drop was used in all. In both cases, the maximum sheath thickness is seen to decrease as the magnetic field incidence angle is increased. Figure 3 shows that at 70° the sheath surrounds only a small portion of the wall. From Figure 5, we also see that the sheath has reduced in maximum thickness by 70% from the value obtained at 0°. A sharp decrease in thickness at $\theta > 70°$ indicates the onset of a sheath collapse. The sheath thickness obtained in the presence of magnetic mirror generally follows the trend of pure field inclination. The slight increase in the thickness with the mirror may be purely a simulation artifact due to the larger domain dimension in the presence of the mirror. The sheath is seen to start collapsing at angles greater than 70°, confirming the simple analysis presented in the introduction. To better illustrate the dynamics at this highly inclined magnetic field geometry, we plot ion velocity contours and velocity streamlines at the 85° incidence angle. This result is shown in Figure 7. The contour plot corresponds to the radial velocity component normalized by the Bohm speed. We see that at this high incidence angle, the value of the normalized velocity remains below unity, indicating that the Bohm speed is never reached. In addition, ions are moving towards the wall only along a small region near the left boundary. This result is likely a direct byproduct of our loading scheme since it affects only the ions injected into the sheath. Ions originating in the bulk plasma are accelerated away from the wall. Ions located just a small distance from the wall are seen to follow trajectory initially parallel to the wall and subsequently turning away from it. Ions are thus seen to be repelled by the wall, indicating a sheath collapse.

B. Erosion and lifetime

Our numerical results confirm that the presence of highly inclined magnetic fields results in a decreased sheath

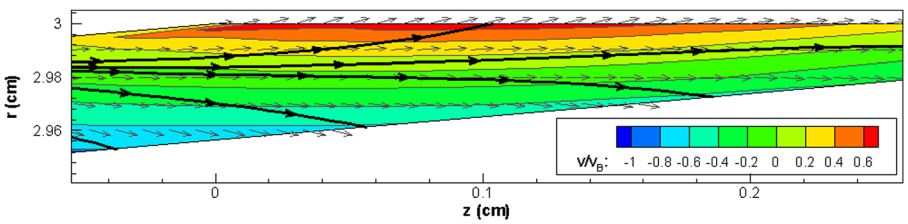

FIG. 7. Plots of normalized radial velocity and ion velocity streamlines at $\theta = 85°$.

thickness. We next correlate this observation to the wall flux. From mass conservation, $\Gamma_w = n_{i,s}u_B$, where the terms on the right hand side correspond to the ion density at the sheath edge and the Bohm velocity. We plot the computed wall flux in Figure 8(a). We can see that although the presence of SEE tends to reduce the sheath thickness, it has only a negligible effect on ion wall flux. The flux remains approximately constant for these cases along the wall length, with the slight decrease due to the reduction in bulk ion density due to ion acceleration. The initial spike is an artifact of the loading scheme, as noted previously. The inclined magnetic field is seen to reduce the wall flux considerably, which can be attributed to the net acceleration of ions away from the wall and hence a reduced sheath ion density $n_{i,s}u_B$. This observation has a profound effect on both the ionization efficiency and the thruster lifetime, since ion losses to the walls are a major contributor to both of these inefficiencies. Here, we consider only the impact on wall erosion. Material sputtering yield scales with both the impact angle and the energy of the incoming ions. Several models exist for computing sputter yields for boron nitride, the material typically used in SPT-type Hall thrusters. In this work, we utilize the logarithmic fit suggested by Garnier,[10]

$$Y_0(E) = 0.0156 \ln E - 0.0638. \tag{7}$$

This fit is valid from the energy threshold of 60 eV up to the keV range. In our analysis, we neglect low energy sputtering. For angular dependence of yield, quadratic polynomial fit is recommended by Yim.[11]

$$Y(E,\theta) = Y_0[-4.45 \times 10^{-7}\theta^4 + 4.91 \times 10^{-5}\theta^3 - 9.72 \times 10^{-4}\theta^2 + 3.44 \times 10^{-3}\theta + 1], \tag{8}$$

where θ is in degrees and is measured from the wall normal.

Figure 8(b) shows the calculated sputter yield. The profiles for the baseline and SEE configurations are shown to exhibit an increase in sputter yield in the axial direction even though the flux decreases. This response is due to the angular dependence. From Figure 3(a), we can see that the ion incidence angle θ increases with the distance along the wall. Similar response is seen in the remaining cases. Presence of a 40° magnetic field inclination results in flux reduction by approximately 60%, leading to a correspondingly similar reduction in erosion rate. In addition, we see that the magnetic mirror has only a marginal effect on wall flux and erosion rates in the inclined field configuration. This can be explained by realizing that both the magnetic field incidence angle and the magnetic mirror generate analogous electric field profiles.

C. Sheath stability

The analysis presented in the previous paragraphs was performed using the prescribed normal component of electric field $E_\perp = 20$ kV/m. Although the actual profile of the potential drop in the Hall thruster adjusts in response to the internal plasma dynamics, the total potential drop is a design parameter arising from the applied potential drop between the anode and the cathode. To investigate the effect, the field strength has on the sheath profile, we ran the code for several values of $E_\perp$ with $\theta = 60°$, no SEE and no magnetic mirror. These results are plotted in Figure 9. The solid line at 20 kV/m corresponds the case studied previously. Reducing the applied potential drop leads to a thicker sheath, as expected. We can see that for this particular field angle, full sheath collapse will occur approximately at $E_\perp = 50$ kV/m. It should be pointed out that this model predicts that the inclined magnetic field leads to sheath formation only if axial electric field is small. According to this model, it is predicted that the potential drop inside the Hall thruster channel decreases leading to shifting the potential drop outside. Such effect has significant implications on the plume formation and the thruster contamination aspects. It is interesting to point out that such trend is also observed experimentally.[12–14]

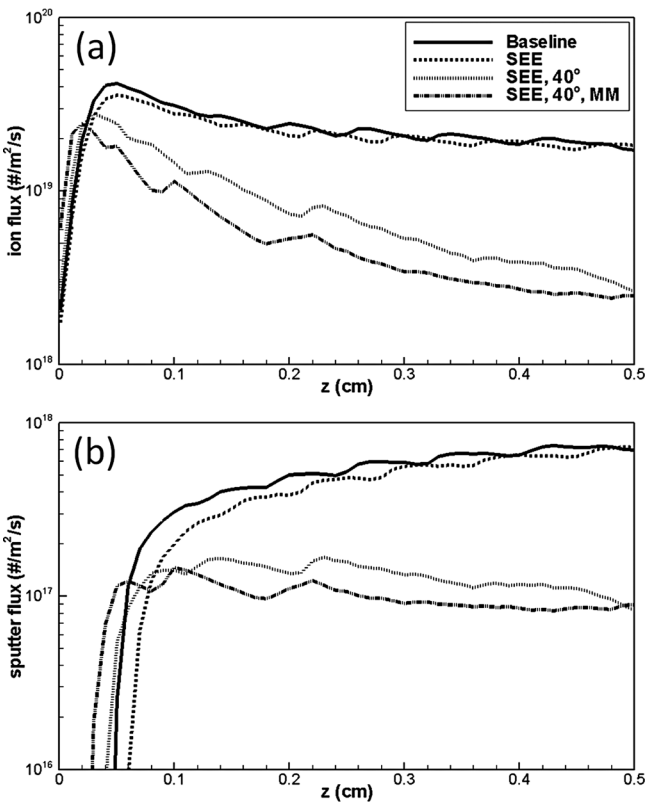

FIG. 8. Comparison of wall flux and computed sputtered yield for 4 selected configurations.

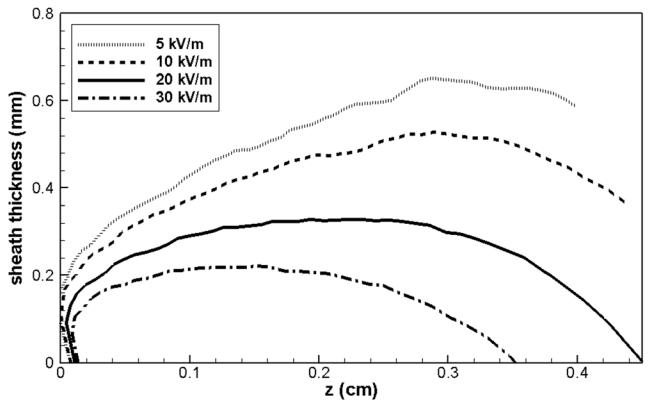

FIG. 9. Sheath profile for $\theta = 60°$ as a function of normal electric field.

V. CONCLUSION

In this paper, we investigated the topology of the plasma sheath that forms along the wall in the acceleration zone of a Hall thruster in the presence of a two dimensional magnetic field. We performed the analysis using a two-dimensional particle-in-cell code. The computation domain consisted of a small near-wall region, allowing us to resolve the Debye length and hence compute potential by solving the Poisson's equation. We studied the effect an increasing angle of magnetic field incidence plays on the near-wall ion dynamics. It was shown that magnetic field incidence angle plays a critical role, and that at highly inclined angles, ions are repelled by the wall leading to a sheath collapses. In addition, we studied the effect of secondary electron emission and magnetic mirror. SEE was shown to have only a negligible effect on wall flux, and magnetic mirror had only a marginal effect on wall fluxes in the inclined field configuration. We used the computed wall fluxes along with an erosion model to predict the effect the magnetic field topology has on thruster lifetime. The erosion rate was seen to decrease by almost one order of magnitude with increase of the incident field to 40°.

ACKNOWLEDGMENTS

The authors would like to thank Shaunak Pai and Yitzy Dachman for assistance with code development and data analysis. This work was supported by Air Force Office of Scientific Research (AFOSR) Grant No. FA9550-10-1-0188. Dr. Mitat Birkan is the grant monitor.

[1]Y. Raitses and N. J. Fisch, "Parametric investigation of a nonconventional Hall thruster," Phys. Plasmas **8**, 2579 (2001).
[2]B. M. Reid and A. D. Gallimore, "Plasma potential measurements in the discharge channel of a 6-kW Hall thruster," in 44th AIAA Joint Propulsion Conference, Hartford, CT, 2008.
[3]A. Fruchtman and A. Cohen-Zur, "Plasma lens and plume divergence in the Hall thruster," Appl. Phys. Lett. **89**, 111501 (2006).
[4]M. Keidar and I. I. Beilis, "Sheath and boundary conditions for plasma simulations of a Hall thruster," Appl. Phys. Lett. **94**, 191501 (2009).
[5]M. Keidar, I. D. Boyd, and I. I. Beilis, "Plasma flow and plasma-wall transition in Hall thruster channel," Phys. Plasmas **8**, 5315 (2001).
[6]D. Sydorenko, A. Smolyakov, I. Kaganovic, and Y. Raitses, "Modification of electron velocity distribution in bounded plasmas by secondary electron mission," IEEE Trans. Plasma Sci. **34**(3), 815 (2006).
[7]M. Lampe, G. Joyce, W. M. Manheimer, and S. P. Slinker, "Quasi-neutral particle simulation of magnetized plasma discharges: General formalism and application to ECR discharges," IEEE Trans. Plasma Sci. **26**(6), 1592 (1998).
[8]M. Keidar and I. D. Boyd, "On the magnetic effect in Hall thrusters," Appl. Phys. Lett. **87**, 121501 (2005).
[9]A. Dunaevsky, Y. Raitses, and N. J. Fisch, "Secondary electron emission from dielectric materials of a Hall thruster with segmented electrodes," Phys. Plasmas **10**, 2574 (2003).
[10]Y. Garnier, V. Viel, J. F. Roussel, and J. Bernard, "Low-energy xenon ion sputtering of ceramics investigated for stationary plasma thrusters," J. Vac. Sci. Technol. A **17**, 3246 (1999).
[11]J. T. Yim, M. Keidar, and I. D. Boyd, "A hydrodynamic-based erosion model for Hall thrusters," in 29th International Electric Propulsion Conference, Princeton, NJ, 2005.
[12]Y. Raitses, D. Staack, M. Keidar, and N. J. Fisch, "Electron-wall interaction in Hall Thrusters," Phys. Plasmas **12**, 057104 (2005).
[13]J. A. Linnell and A. D. Gallimore, "Internal plasma potential measurements of a Hall thruster using plasma lens focusing," Phys. Plasmas **13**, 103504 (2006).
[14]Y. Raitses, A. Smirnov, and N. J. Fisch, "Effects of enhanced cathode electron emission on Hall thruster operation," Phys. Plasmas **16**, 057106 (2009).